ACS APPLIED MATERIALS & INTERFACES

www.acsami.org

Research Article

Ultrasensitive Detection of Amyloid β Oligomers Based on the "DD−A" FRET Binary Probes and Quadrivalent Cruciform DNA Nanostructure-Mediated Cascaded Amplifier

Yuanyuan Zhang, Jinwen Zhao, Guomin Yang, Ying He, Shihong Chen,* and Ruo Yuan

Cite This: *ACS Appl. Mater. Interfaces* 2021, 13, 32013−32021

Read Online

ACCESS | Metrics & More | Article Recommendations | Supporting Information

ABSTRACT: The reported donor donor−acceptor ("DD−A") fluorescence resonance energy transfer (FRET) was typically achieved through random collisions and interactions of DNA molecules in the bulk solution, which has inevitable defects, including weak biological stability, slow reaction kinetics, and low hybridization efficiency. In order to overcome these deficiencies, this work developed a quadrivalent cruciform DNA nanostructure (qCDN)-mediated cascaded catalyzed hairpin assembly (CHA) amplifier for the fluorescence detection of amyloid β oligomer species (AβOs). First, four H1 and four H2 hairpins were assembled on one qCDN to obtain qCDNH1 and qCDNH2, respectively. In the presence of AβOs, strand C was released from the P1−C hybrid hairpin and then alternately opened qCDNH1 and qCDNH2 to trigger the qCDN-mediated CHA. As a result, double donors in H1 and one acceptor in H2 were mutually closed, and the porous DNA nanonet with a high loading of "DD−A" FRET binary probes was formed. The FRET efficiency was approximately 78%, and the initial reaction rate was 25-fold faster than the conventional CHA. The detection limit of AβOs was as low as 0.69 pM. The combination of the "DD−A" FRET binary probes and qCDN-mediated cascaded amplifier exhibited great promise for detecting biomarkers with trace levels.

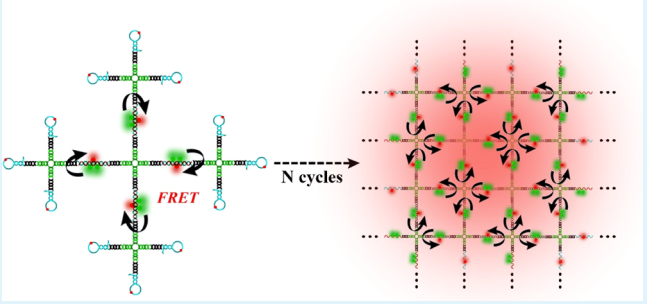

KEYWORDS: *amyloid β oligomer, ratiometric biosensor, fluorescence resonance energy transfer, catalyzed hairpin assembly, cruciform DNA nanostructure*

1. INTRODUCTION

Over the past decades, the fluorescence resonance energy transfer (FRET) technique has been gradually developed as a mature method for detecting a variety of biological molecules due to its simple design, short time consumption, and easy operation.[1,2] Moreover, it could effectively eliminate systematic fluctuation, decrease the risk of false-positives, and provide built-in corrections for environmental impacts through recording the intensity ratio of two fluorescence emissions rather than a single fluorescence intensity.[3,4] For example, Chen et al. constructed a DNA dendrimer for the ultrasensitive detection of lead ions based on the FRET between fluorophores FAM and TAMRA.[5] Wang's group designed an upgraded FRET nanoflare for the ratiometric detection of intracellular miRNA in living cells.[6] However, those reported donor−acceptor ("D−A") FRET technologies exhibited a relatively poor FRET efficiency, thus resulting in a low detection sensitivity. Contrasted with the conventional "D−A" systems, the donor donor−acceptor ("DD−A") FRET mode makes two adjacent fluorescent donors (FAM) and one fluorescent acceptor (TAMRA) close to each other, and then, energy transfer occurred through intermolecular resonance to generate a significant FRET signal. The "DD−A" FRET mode could remarkably enhance the FRET efficiency, thus attracting the attention of researchers. For example, Wang et al. developed a MnO_2 nanosheet-mediated "DD−A" FRET signal mechanism for detecting miRNA.[7] However, the corresponding hybridization reaction occurred by random collisions and interactions of DNA molecules in bulk solutions, which would encounter problems, such as weak biological stability, slow reaction kinetics, and low hybridization efficiency. Therefore, it is highly demanded to improve the biological stability and reaction kinetics of the "DD−A" FRET system.

Due to the excellent biocompatibility, nanoscale controllability, and spatial addressability, DNA nanostructures have turned into promising candidates to enhance biological stability and reaction kinetics and have been widely applied in biosensing, drug delivery, molecular computing, and genetic

Received: April 25, 2021
Accepted: June 17, 2021
Published: July 2, 2021

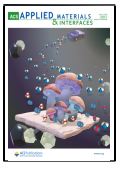

https://doi.org/10.1021/acsami.1c07598
ACS Appl. Mater. Interfaces 2021, 13, 32013−32021

analysis.[8−10] These DNA nanostructures could be expediently constructed by molecular positioning self-assembly with nanometer precision, such as DNA origami,[11] DNA nanogears,[12] DNA nanowires,[13] and so on. For example, Ren et al. proposed a responsive DNA nano string light by the interval hybridization of modified hairpin DNA probe pairs and a DNA nanowire generated by rolling circle amplification,[14] in which expensive and erratic proteases and complex experimental operations were involved. Qing et al. developed a DNA tetrahedron based on intramolecular catalytic hairpin assembly [intra-catalyzed hairpin assembly (intra-CHA)] to increase reaction kinetics and signal stability for miRNA detection.[15] Although the employment of proteases was averted, the reported intra-CHA amplifier had only two hairpin probes labeled on a DNA tetrahedron for FRET signal amplification, thus exhibiting an unsatisfactory amplification efficiency. More significantly, the DNA nanostructure-mediated "DD−A" model has not been reported yet. The development of a nonenzymatic and highly efficient DNA nanostructure-mediated "DD−A" FRET is of great value.

Alzheimer's disease (AD) is the most severe neurodegenerative disease facing the world today. Its clinical manifestations are amyloid plaques appeared in brain tissue slices, neuronal death, impaired cognition and memory abilities, and severe damaged brain function.[16,17] It is now widely accepted that the soluble amyloid β oligomer species (AβOs) are the most neurotoxic forms in human cerebrospinal fluid (CSF).[18−20] AβOs were generally accumulated at a very early stage of the disease, and their levels change 10−15 years earlier than the clinical symptoms, which are considered to be one of the specific biomarkers for the early diagnosis of AD.[21] Therefore, monitoring the subtle levels of AβOs in CSF is efficacious for predicting the severity and progress at the early or preclinical stages of AD.

Herein, we designed a quadrivalent cruciform DNA nanostructure (qCDN)-mediated cascaded CHA amplifier to improve the biological stability, reaction kinetics, and hybridization efficiency of the current "DD−A" FRET model for detecting AβOs. Four hairpin probes H1 (labeled with two fluorophores FAM as FRET donors) and four hairpin probes H2 (labeled with a fluorophore TAMRA as the FRET acceptor) were assembled at the tail end of qCDN via base complementary pairing, respectively, resulting in the formation of qCDNH1 and qCDNH2. Because the four tail ends in the qCDN were apart from each other, the high steric hindrance caused by the dense DNA nanostructure could be effectively avoided. In the presence of target AβOs, strand C released from the P1−C hybrid hairpin could not only promote the cyclic use of target AβOs but also alternately open qCDNH1 and qCDNH2 to efficiently trigger the qCDN-mediated cascaded CHA. Thus, a large number of qCDNH1−qCDNH2 complexes were formed and double FAM and single TAMRA were mutually closed in qCDNH1−qCDNH2 complexes, resulting in a significant decrease in the fluorescence intensity from FAM and a significant increase in the fluorescence intensity from TAMRA. Due to the synergistic effect of multiple reaction directions, the collision probability is greatly increased, and the local concentration is significantly enhanced, which dramatically accelerates the reaction kinetics and effectively improves the hybridization efficiency. The integration of the qCDN-mediated cascaded CHA amplifier and "DD−A" FRET mode provides a promising fluorescence platform and a new method for monitoring trace amounts of AβOs.

2. EXPERIMENTAL SECTION

2.1. Reagents, Materials, and Apparatus. Detailed information on the materials, reagents, and apparatus used in this work is presented in the Supporting Information. The sequences and modifications of DNA oligonucleotides are listed in Table S1.

2.2. Preparation of Soluble AβOs. The lyophilized powder of Aβ_{1-40} was dissolved in 1.0 mg/mL hexafluoroisopropanol (HFIP) and sonicated for 10 min. The resultant monomers of Aβ_{1-40} were incubated overnight at room temperature. Next, HFIP was evaporated under a gentle stream of high-purity nitrogen flow to obtain the Aβ solution, which was redissolved in dimethyl sulfoxide to obtain Aβ monomer species (AβMs). AβMs were stored in a refrigerator at −20 °C for later use. The AβOs were prepared by incubating AβMs for a given time at 37 °C and then diluted with phosphate-buffered saline buffer (2.0 mM, pH 7.4) to the desired concentration for the experiment. The calculated concentration of AβOs was equivalent to the concentration of AβMs.

2.3. Construction of the qCDN-Assembled Hairpin Structure. The DNA stock solutions (0.10 mM) were prepared in RNAase-free ultrapure water and further diluted to a certain concentration using TE buffer (pH 8.0). 10.0 μL of cruciform DNA was prepared by annealing the mixture of Y1, Y2, Y3, and Y4 (4.0 μM and 2.5 μL for each) at 95 °C for 5 min and subsequently cooling to 25 °C for 120 min. Meanwhile, H1 and H2 were respectively annealed by the method described above to form a stem-loop structure. Then, the annealed H1 (10.0 μL, 4.0 μM) and H2 (10.0 μL, 4.0 μM) reacted with the as-prepared cruciform DNA (10.0 μL, 1.0 μM) at 37 °C for 120 min to form qCDNH1 and qCDNH2, respectively.

2.4. Analytical Protocol for the Cascade Amplified Fluorescence Detection of AβOs. Prior to experiments, the hairpin aptamer probe (HAP) and hairpin P1 were respectively annealed at 95 °C for 5 min and then cooled to 25 °C for 120 min to form a stable stem-loop structure. Then, 10.0 μL of P1 (4.0 μM) and 10.0 μL of strand C (4.0 μM) were mixed and hybridized at 37 °C for 120 min to yield P1−C hybrids (2.0 μM). Next, 10.0 μL of AβOs with different concentrations and 10.0 μL of HAP (4.0 μM) were incubated for 120 min at 37 °C. Afterward, the as-prepared P1−C hybrids (20.0 μL, 2.0 μM), qCDNH1 (20.0 μL, 1.0 μM), and qCDNH2 (20.0 μL, 2.0 μM) were introduced into the above-mentioned mixture solution for further hybridizing at 35 °C for 120 min. Finally, the fluorescence measurements were performed on the obtained solutions.

2.5. Native Polyacrylamide Gel Electrophoresis. First, 10.0 μL of different DNA samples was mixed with 2.0 μL of 6× loading buffer solutions for dyeing. Then, the dyed DNA solution (12.0 μL) and DNA marker solution (6.0 μL) were moved into notches of the freshly prepared native polyacrylamide gel (16 and 8%, respectively). Gel electrophoresis was implemented in the electrophoretic buffer solution (1× TBE, pH 8.0) at a 120 V constant voltage. When the staining solution reached about 1 cm from the bottom edge of the gel plate, the electrophoresis experiment was stopped. Subsequently, the resultant gel was stained with GR001 Real Red nucleic acid dye (GelRed) for 15 min and finally transferred to the Gel Doc XR+ System for gel imaging to obtain the electrophoresis results.

2.6. Fluorescence Measurements. The fluorescence measurements were carried out at an excitation wavelength of 496 nm. The fluorescence emission spectrum data were collected from 510 to 650 nm at 5 nm of slit widths for the excitation and emission at 950 V PMT voltage. The ratio of the fluorescence intensity from TAMRA at 580 nm (F_A) to the fluorescence intensity from FAM at 520 nm (F_D), namely, the FRET ratio (F_A/F_D), was computed to evaluate the response performance.

https://doi.org/10.1021/acsami.1c07598
ACS Appl. Mater. Interfaces 2021, 13, 32013−32021

Scheme 1. Schematic Illustration of (A) the Formation of qCDNH1 and qCDNH2, (B) Recycling Process of Target AβOs, and (C) CHA Recycling Triggered by Strand C for the Dynamic Self-Assembly of the DNA Nanonet

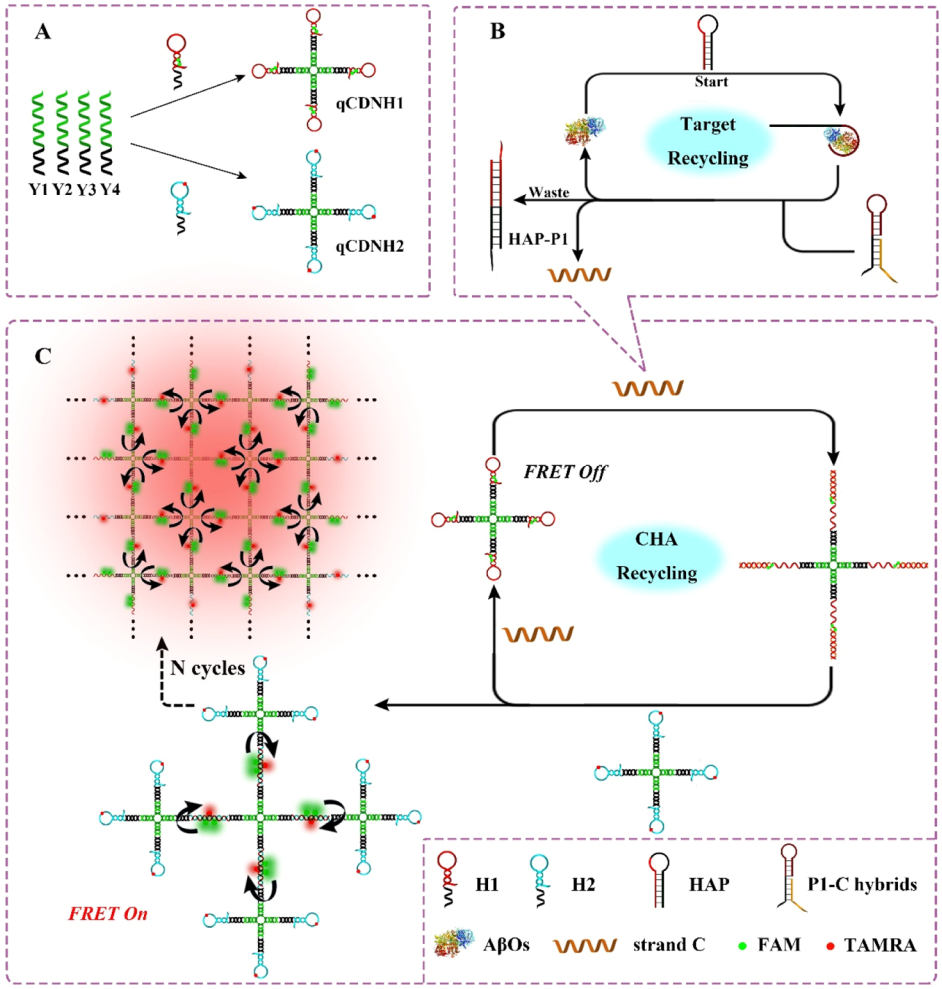

3. RESULTS AND DISCUSSION

3.1. Principle of the Designed Strategy. The principle of our designed "DD−A" FRET mechanism and qCDN-mediated cascaded CHA amplification strategy for detecting AβOs is illustrated in Scheme 1. As shown in Scheme 1A, four oligonucleotides (Y1, Y2, Y3, and Y4) were mixed to form qCDN because of their mutual hybridization. Four H1 hairpins were assembled on a qCDN to obtain qCDNH1 because each of four A9C6 tails of a qCDN hybridized with the T9G6 tail of H1. In the same way, four H2 hairpins with T9G6 tails were assembled on a qCDN with four A9C6 tails to obtain qCDNH2. In the absence of AβOs, HAP maintained a stable hairpin structure and strand C was hybridized stably with hairpin P1, thus the CHA cascade amplification reaction could not be triggered and the FRET between FAM and TAMRA could not occur. In this case, a high fluorescence intensity for donor FAM and a low fluorescence intensity for acceptor TAMRA were detected. In the presence of target AβOs, AβOs would combine with the aptamer segment of HAP to form a tight structure due to the high binding affinity between them (Scheme 1B). Subsequently, the newly exposed sequence of HAP hybridized with the black region of P1−C and opened the P1−C hybrids through branch migration, resulting in the liberation of the target AβOs as well as strand C at the same time. The released AβOs were used cyclically to combine with the aptamer segment of HAP to liberate strand C. With the target recycling, plenty of strand C was liberated. The released strand C hybridized with qCDNH1 via the toehold-mediated strand-displacement reactions to form the C-qCDNH1 intermediate. Next, the toehold of qCDNH2 would hybridize with the newly exposed segment of the C-qCDNH1 intermediate and then displace the strand C through strand migration (Scheme 1C). Since the released strand C could act as a catalyst to trigger CHA recycling, a large number of qCDNH1−qCDNH2 complexes were formed and double FAM and single TAMRA were mutually closed in qCDNH1−qCDNH2 complexes, resulting in a significant decrease in the fluorescence intensity from FAM and a significant increase in the fluorescence intensity from TAMRA due to the FRET. Through such a qCDN-mediated cascaded CHA amplification strategy, the qCDNH1−qCDNH2 complexes would self-assemble to form a straticulate and porous DNA nanonet with a high loading of "DD−A" FRET binary probes, leading to a substantially improved FRET efficiency for the highly sensitive detection of AβOs.

The "DD−A" FRET mechanism and qCDN-mediated cascaded CHA amplification strategy had the following advantages. First, because the four tail ends in the qCDN were apart from each other, the high steric hindrance caused by the dense DNA nanostructure could be effectively avoided, which was beneficial for the formation of the straticulate and

https://doi.org/10.1021/acsami.1c07598
ACS Appl. Mater. Interfaces 2021, 13, 32013−32021

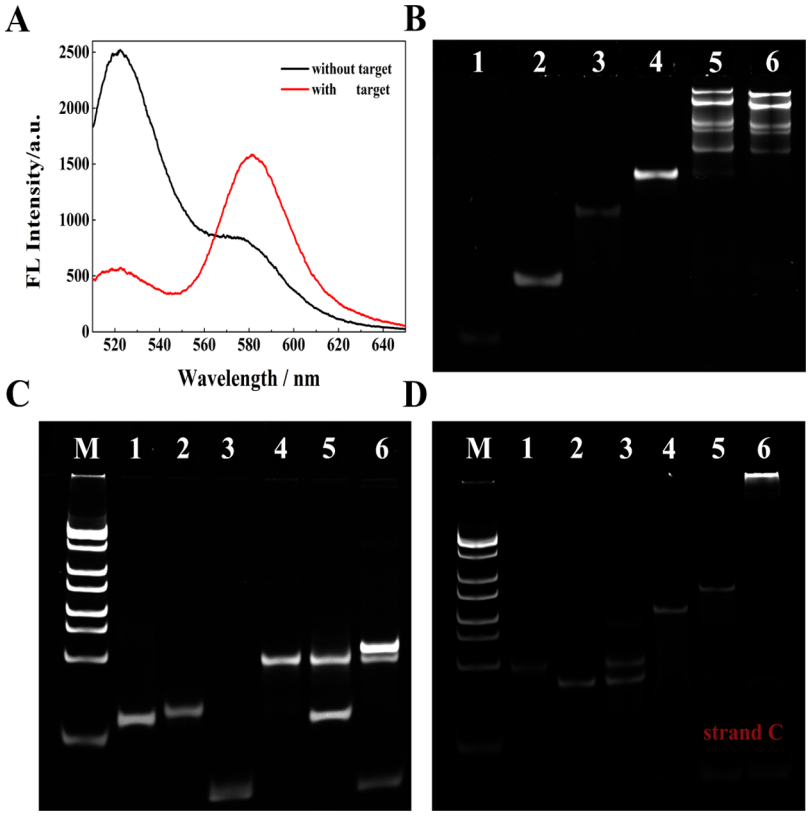

Figure 1. (A) Fluorescence emission without and with target AβOs. (B) Native PAGE (8%) images for Y1 (lane 1), Y1 + Y2 (lane 2), Y1 + Y2 + Y3 (lane 3), Y1 + Y2 + Y3 + Y4 (lane 4), qCDNH1 (lane 5), and qCDNH2 (lane 6). (C) Native PAGE (16%) images of the target recycling process, DNA marker (lane M), HAP (lane 1), P1 (lane 2), strand C (lane 3), P1−C hybrids (lane 4), HAP + P1−C hybrids (lane 5), and AβOs + HAP + P1−C hybrids (lane 6). (D) Native PAGE (16%) images of the CHA recycling process, DNA marker (lane M), H1 (lane 1), H2 (lane 2), H1 + H2 (lane 3), H1 + strand C (lane 4), H1 + H2 + strand C (lane 5), and qCDNH1 + qCDNH2 + strand C (lane 6). The concentrations of AβOs, HAP, P1, strand C, H1, and H2 were 100, 500, 500, 500, 250, and 500 nM, respectively.

porous DNA nanonet. Second, each qCDNH1 and qCDNH2 contained four hairpin probes, which were located in different orientations, resulting in the improvement of the collision probability between H1 and H2 in the two-dimensional cruciform DNA nanostructure. Third, once one hairpin H1 or H2 at the tail end of the qCDN participated in the cascaded CHA reaction, the other three hairpin probes on the same qCDN were naturally entered into the two-dimensional DNA nanonet, thereby greatly increasing the local concentrations of H1 and H2 in qCDN. More importantly, the "DD−A" FRET mechanism made two fluorescence donors and one fluorescence acceptor proximity close, which greatly improved FRET efficiency and detection sensitivity.

3.2. Characterization of the Cascade Amplified Strategy. To demonstrate the feasibility of the "DD−A" FRET mechanism and qCDN-mediated cascaded CHA amplification strategy for AβOs detection, the fluorescence intensity was detected with and without the target AβOs, respectively. As seen from Figure 1A, in the presence of the target AβOs, the fluorescence intensity from donor FAM at 520 nm greatly decreased and the fluorescence intensity from acceptor TAMRA at 580 nm significantly increased, suggesting a strong FRET signal.

The native polyacrylamide gel electrophoresis (PAGE) experiments were carried out to further verify the feasibility of the proposed amplified strategy. First, 8% PAGE experiment was implemented to confirm the assembly of qCDNH1 and qCDNH2, and the results are depicted in Figure 1B. With the successive addition of DNA strands Y1, Y2, Y3, and Y4, a stepwise decrease in the gel electrophoretic rate was observed from lane 1 to lane 4, which demonstrated the successful formation of the qCDN. While H1 and H2 reacted with the qCDN for 120 min to obtain qCDNH1 and qCDNH2, respectively, the new bright band with very slow mobility at the top in lane 5 and lane 6 indicated the successful preparation of qCDNH1 and qCDNH2.

Next, 16% PAGE experiments were performed to verify the feasibility of target recycling. As shown in Figure 1C, the intact HAP, P1, and strand C displayed their own gel electrophoretic mobility (from lane 1 to lane 3). The new band was clearly observed in lane 4, while P1 was combined with strand C, indicating the formation of P1−C hybrids. When HAP was mixed with P1−C hybrids (lane 5), two separate bands were clearly observed, which corresponded to the bands of lane 1 and lane 4, suggesting that the target recycling could not be triggered without the target AβOs. When the target AβOs was incubated with the mixture of HAP and P1−C hybrids (lane 6), a bright band at the bottom was observed, which corresponded to the band of pure strand C, indicating that the target recycling was initiated by the AβOs and strand C was liberated.

Subsequently, the feasibility of CHA recycling was verified by 16% PAGE experiments. Due to the huge difference in the relative molecular weights of qCDNH1 and strand C, the CHA recycling process cannot be perfectly presented on a gel image. Therefore, H1 and H2 were used to replace qCDNH1 and

https://doi.org/10.1021/acsami.1c07598
ACS Appl. Mater. Interfaces 2021, 13, 32013−32021

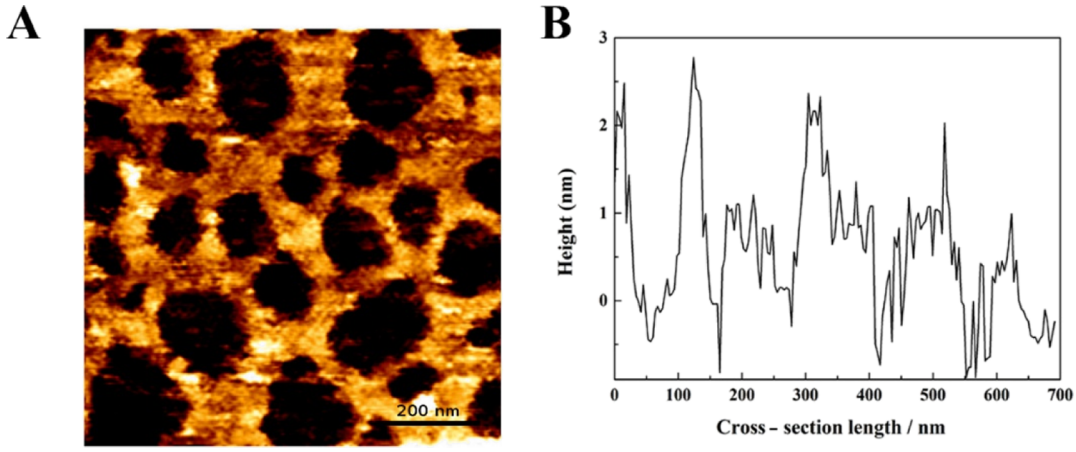

Figure 2. (A) AFM characterization of the DNA nanonet and (B) relevant height profile of the DNA nanonet.

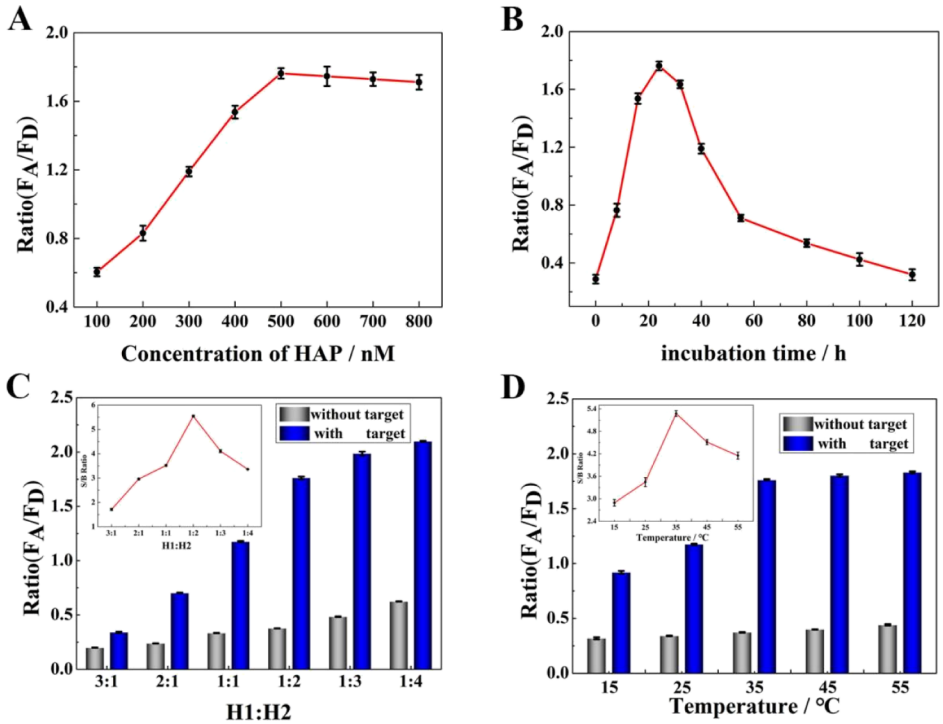

Figure 3. Influence of (A) HAP concentration, (B) incubation time for AβMs to form AβOs, (C) concentration ratio of H1 and H2, and (D) reaction temperature of target recycling and CHA recycling on the FRET ratio (F_A/F_D). The detection solution contains 1 nM AβOs, 500 nM HAP, 500 nM P1, 500 nM strand C, 250 nM H1, and 500 nM H2.

qCDNH2 to verify the feasibility of CHA recycling. The corresponding results are depicted in Figure 1D. Lane 1 and lane 2 stood for the hairpins H1 and H2, respectively. No new band was displayed for the mixture of H1 and H2 (lane 3), suggesting that there is no spontaneous assembly between H1 and H2, just as there is no spontaneous assembly between qCDNH1 and qCDNH2. When H1 was mixed with strand C, a new band appeared in lane 4, indicating the formation of C−H1 hybrid complexes, just as the formation of the C−qCDNH1 intermediate. The new band with very slow mobility in lane 5 indicated that the CHA recycling was triggered by strand C to form the H1−H2 duplexes. Also, the new bright band with a very slow gel electrophoretic rate at the top in lane 6 indicated that the CHA recycling was triggered by strand C to form the qCDNH1−qCDNH2-mediated nanonet.

Atomic force microscopy (AFM) was also used for the characterization of our proposed qCDN-mediated nanonet. As shown in Figure 2A, a perfect porous DNA nanonet was clearly observed. The relevant height profile (Figure 2B) demonstrated that its height was consistent with the relevant height of DNA. The AFM image and relevant height profile demonstrated that the qCDN-mediated nanonet structure was successfully formed.

All of the above-mentioned results illustrated the feasibility of our designed "DD−A" mode and qCDN-mediated cascaded CHA amplification strategy for AβOs detection.

3.3. Optimization of the Experimental Conditions. A series of experimental conditions were optimized, including the concentration of HAP, the incubation time for AβMs to form AβOs, the concentration ratio of H1 and H2, and the reaction temperature of target recycling and CHA recycling. The

https://doi.org/10.1021/acsami.1c07598
ACS Appl. Mater. Interfaces 2021, 13, 32013−32021

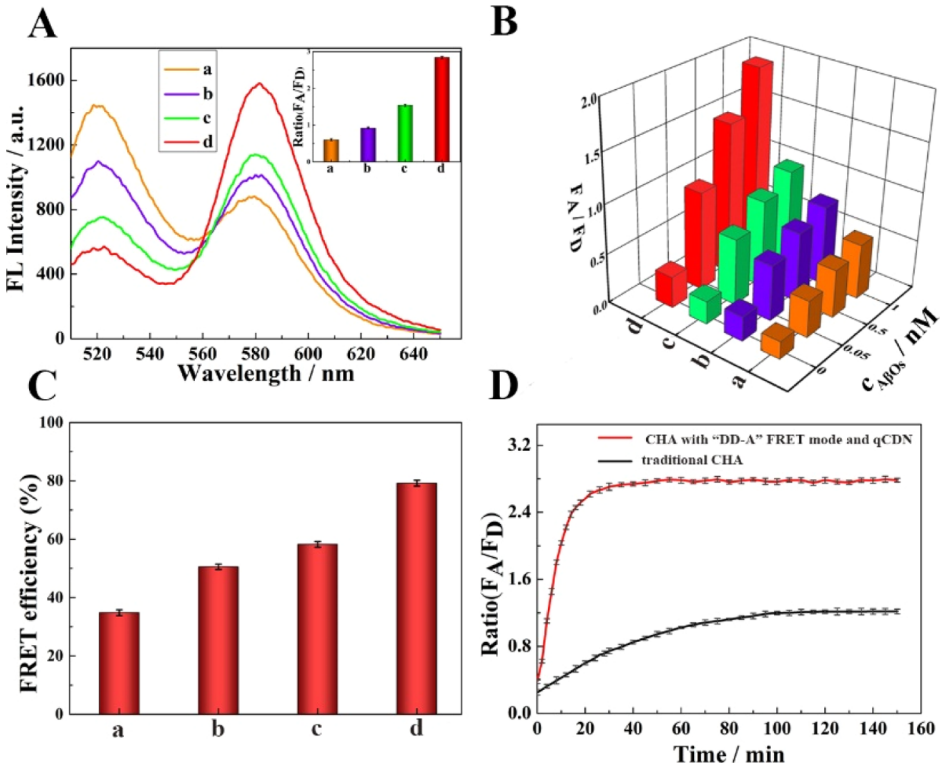

Figure 4. (A) Fluorescence emission spectra of probe (a), probe (b), probe (c), and probe (d); inset: the FRET ratio signal (F_A/F_D) of the four FRET probes. (B) Fluorescence response of four FRET probes to different concentrations of the target AβOs. (C) FRET efficiencies of four FRET probes. (D) Real-time fluorescence spectra of CHA with the "DD−A" FRET mode and qCDN [probe (d)] and traditional CHA [probe (a)]. The detection solution contains 100 nM AβOs, 500 nM HAP, 500 nM P1, 500 nM strand C, 250 nM H1, and 500 nM H2.

hairpin HAP was a vital component of the target recycling, and its concentration would directly influence the response performance of the proposed sensor. A moderate amount of HAP was beneficial to the target recycling, while an excessive amount would result in its waste. Therefore, the optimization of the concentration of HAP was essential. As shown in Figure 3A, when the concentration of HAP shifted from 100 to 800 nM, the FRET ratio (F_A/F_D) gradually increased and reached the maximum at 500 nM. Herein, 500 nM was chosen as the optimal concentration of HAP for the following detection.

The AβOs were prepared by incubating AβMs for a given time at 37 °C. With the increase of the incubation time, AβMs could combine to form AβOs and further reorganize and aggregate into Aβ fibril species (AβFs), but the hairpin HAP only had high specific binding to AβOs. Therefore, it is crucial to optimize the incubation time for AβMs to form AβOs. As seen from Figure 3B, the FRET ratio increased with the increase of the incubation time for AβOs formation in the range of 1−25 h and began to decrease beyond 25 h. Thus, the optimal incubation time for AβMs to form AβOs was 25 h.

The developed "DD−A" FRET mode involved two fluorophores FAM in H1 and one fluorophore TAMRA in H2; therefore, the concentration ratio of H1 in qCDNH1 and H2 in qCDNH2 would affect the FRET efficiency. The ratio of the fluorescence intensity from TAMRA (F_A) to the fluorescence intensity from FAM (F_D) was defined as the FRET ratio (F_A/F_D), and $(F_A/F_D)_1$ and $(F_A/F_D)_0$ were denoted as the FRET ratio (F_A/F_D) with and without the target AβOs, respectively. As seen from Figure 3C, when the concentration ratio of H1 and H2 shifted from 3:1 to 1:4, the FRET ratio $(F_A/F_D)_1$ (blue pillar) significantly increased. In fact, $(F_A/F_D)_0$ (gray pillar) also slightly increased, and it is the ratio $(F_A/F_D)_1/(F_A/F_D)_0$ that really reflected the signal-to-background ratio (S/B). Thus, the effect of the concentration ratio of H1 and H2 on the S/B was further investigated, and the results are depicted in the inset of Figure 3C. As seen, the S/B tended to achieve the maximum, while the concentration ratio reached 1:2. Thus, 1:2 was chosen as the optimal concentration ratio of H1 and H2, which coincided with the results reported by the literature.[22]

The effect of the reaction temperature of the target recycling and CHA recycling on the fluorescence signal was further investigated. As seen from Figure 3D, the FRET ratio was effectively improved by increasing the reaction temperature from 15 to 35 °C and began to decrease beyond 35 °C. Therefore, 35 °C was chosen as the optimal reaction temperature for subsequent assays.

3.4. Amplification Efficiency of the Proposed Strategy. In order to confirm that our constructed FRET probe (CHA with the "DD−A" FRET mode and qCDN) had a high amplification efficiency, three kinds of control probes were constructed for the control experiments, including probe (a) (traditional CHA with the "D−A" FRET mode and without qCDN), probe (b) (CHA with the "D−A" FRET mode and qCDN), and probe (c) (CHA with the "DD−A" FRET mode and without qCDN). First, the fluorescence signal intensities of four types of FRET probes were compared in the case of 100 nM AβOs, and the results are presented in Figure 4A. As expected, our target probe (CHA with the "DD−A" FRET mode and qCDN), namely, probe (d) in Figure 4, showed the strongest FRET signal. The corresponding FRET ratios (F_A/F_D) of the four types of FRET probes were calculated. As

https://doi.org/10.1021/acsami.1c07598
ACS Appl. Mater. Interfaces 2021, 13, 32013−32021

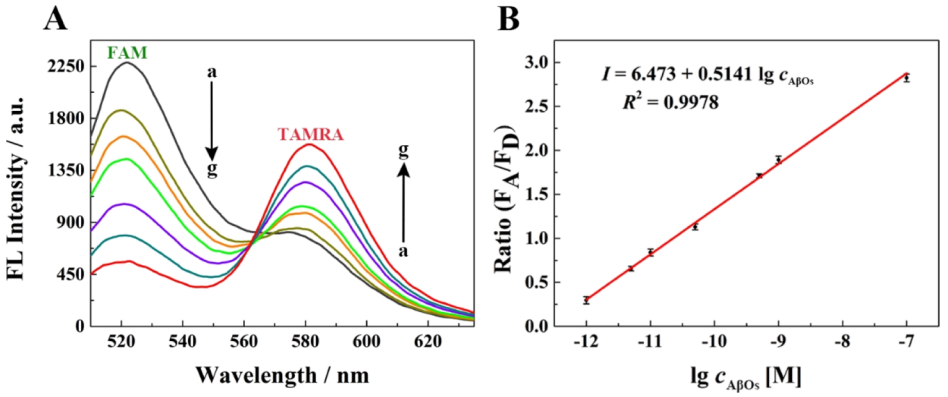

Figure 5. (A) Fluorescence responses of the "DD−A" mode and qCDN-mediated cascaded amplifier for the detection of AβOs at different concentrations: (a) 1, (b) 5, (c) 10, (d) 50, (e) 100 pM, (f) 1, and (g) 100 nM. (B) Calibration curve of the fluorescence intensity and the logarithmic concentration of target AβOs from 1 pM to 100 nM.

shown in the inset of Figure 4, our target probe [probe (d)] exhibited the highest FRET ratio (F_A/F_D). As seen from Figure 4B, when different concentrations of AβOs were added, the FRET ratio (F_A/F_D) of probe d was remarkably increased and was obviously distinguished from other control FRET probes. Additionally, the FRET efficiencies of four FRET probes were calculated,[23] and the results are depicted in Figure 4C. As seen, our target probe [probe (d)] exhibited the highest FRET efficiency, and it was approximately 78%, which has an enhancement of 2.3 fold than traditional CHA [probe (a)]. Finally, time-dependent fluorescence analysis was implemented to investigate the reaction kinetics. The comparison between our target probe [CHA with the "DD−A" FRET mode and qCDN, namely, probe (d)] and the traditional CHA [probe (a)] was performed by monitoring the FRET ratio signal (F_A/F_D). As shown in Figure 4D, probe (d) could rapidly respond to 100 nM of the target AβOs and the reaction speed was dramatically accelerated. The completion time of CHA with the "DD−A" FRET mode and qCDN [probe (d)] was about 24 min, which was 4.38 times shorter than the traditional CHA [probe (a)]. Compared with the slope of real-time fluorescence analysis curves, the initial reaction rate of our target probe [probe (d)] was 25-fold faster than traditional CHA [probe (a)]. Thus, our proposed strategy had a high amplification efficiency for the detection of the AβOs.[24−32]

3.5. Performance of the Proposed Biosensing Platform toward AβOs. Under the optimized experimental conditions, the detection of target AβOs was performed using our proposed strategy. Figure 5A depicts the change of the fluorescence emission intensity with the target AβOs. As seen, the fluorescence intensity from FAM (donor) at 520 nm was reduced promptly with the increasing concentrations of AβOs, while the fluorescence emission intensity from TAMRA (acceptor) at 580 nm was increased accordingly. The FRET ratios (F_A/F_D) at different target concentrations were calculated, and the relationship between F_A/F_D and the concentration of AβOs is shown in Figure 5B. A good linear correlation between the FRET ratio and the logarithm of AβOs concentrations was observed. The linear equation is $I = 0.5141 \lg c_{A\beta Os} + 6.473$, where I is the FRET ratio (F_A/F_D) and $c_{A\beta Os}$ is the concentration of AβOs. The detection limit was evaluated to be 0.69 pM at a signal-to-noise ratio (S/N) of 3. The FRET ratio (F_A/F_D) increased from 0.31 to 2.75 when the concentration of the target AβOs shifted from 1 pM to 100 nM, indicating a nearly 8.87-fold enhancement in the FRET ratio. Compared with other reported detection methods for AβOs, our proposed fluorescence biosensor showed better performance, as listed in Table S2.

3.6. Specificity Investigation and Practical Application of the Proposed Amplified Strategy. To assess the specificity of the proposed fluorescence detection platform, AβMs, AβFs, carcinoembryonic antigen, alpha fetoprotein, and ferritin were chosen as interfering substances. The results are presented in Figure S1. As compared to the blank, no significant fluorescence response was observed for the above-mentioned five interfering substances when their concentrations were 100 times higher than that of the target AβOs. However, both the target AβOs and the mixture of AβOs and the above-mentioned five interfering substances exhibited a significant enhancement in the fluorescence signal, suggesting an excellent specificity of our proposed fluorescence platform for AβOs detection.

In order to explore the practical application of our proposed strategy for AβOs detection in real samples, the fluorescence recovery tests were performed through the standard addition method with artificial CSF (ACSF)[19] and 50-fold diluted serums as real samples. The results are presented in Table 1.

Table 1. Recovery Rates of AβOs in ACSF and Serum

sample	no.	c_{added}/nM	$c_{detected}$/nM[a]	recovery %	RSD %
ACSF	1	0.100	0.0970	97.30	1.7
	2	2.00	2.14	106.9	2.3
	3	10.0	10.7	103.4	4.1
serum	1	0.100	0.101	101.0	2.9
	2	2.00	2.05	102.5	3.7
	3	10.0	9.33	93.30	1.1

[a]Average of three determinations.

The recovery rates were in the range of 97.3−106.9 and 93.3−102.5% for the ACSF and serum solution, respectively, which indicated that the constructed fluorescence biosensing platform had a great potential application for the detection of AβOs in real samples.

4. CONCLUSIONS

In this work, we designed a qCDN-mediated cascaded CHA amplifier and integrated it and the "DD−A" FRET binary probe for detecting AβOs. Such a strategy exhibited remarkable advantages. First, because the four tail ends in

https://doi.org/10.1021/acsami.1c07598
ACS Appl. Mater. Interfaces 2021, 13, 32013−32021

the qCDN were apart from each other, the high steric hindrance caused by the dense DNA nanostructure could be effectively avoided to ensure the formation of the DNA nanonet, which promoted the substantial FRET pair mutually close and displayed an excellent fluorescence performance. More importantly, reaction rates were dramatically accelerated, and hybridization efficiency and FRET efficiency were effectively improved due to the synergistic effect of increased collision probability, multiple reaction orientations, augmented local concentrations, and "DD−A" FRET ratiometric signal outputs. The combination of target recycling amplification, "DD−A" FRET mode, and qCDN-mediated cascaded CHA amplifier provided a promising fluorescence detection platform and a novel method for AβOs detection.

■ ASSOCIATED CONTENT

Supporting Information

The Supporting Information is available free of charge at https://pubs.acs.org/doi/10.1021/acsami.1c07598.

Reagents and materials; apparatus; comparison for the analytical performance of different AβOs detection methods; and specificity investigation of the proposed amplified strategy (PDF)

■ AUTHOR INFORMATION

Corresponding Author

Shihong Chen − *Key Laboratory of Luminescence Analysis and Molecular Sensing (Southwest University), Ministry of Education, College of Chemistry and Chemical Engineering, Southwest University, Chongqing 400715, PR China;* orcid.org/0000-0001-7101-1223; Phone: +86-23-68253172; Email: cshong@swu.edu.cn; Fax: +86-23-68253172

Authors

Yuanyuan Zhang − *Key Laboratory of Luminescence Analysis and Molecular Sensing (Southwest University), Ministry of Education, College of Chemistry and Chemical Engineering, Southwest University, Chongqing 400715, PR China*

Jinwen Zhao − *Key Laboratory of Luminescence Analysis and Molecular Sensing (Southwest University), Ministry of Education, College of Chemistry and Chemical Engineering, Southwest University, Chongqing 400715, PR China*

Guomin Yang − *Key Laboratory of Luminescence Analysis and Molecular Sensing (Southwest University), Ministry of Education, College of Chemistry and Chemical Engineering, Southwest University, Chongqing 400715, PR China*

Ying He − *Key Laboratory of Luminescence Analysis and Molecular Sensing (Southwest University), Ministry of Education, College of Chemistry and Chemical Engineering, Southwest University, Chongqing 400715, PR China*

Ruo Yuan − *Key Laboratory of Luminescence Analysis and Molecular Sensing (Southwest University), Ministry of Education, College of Chemistry and Chemical Engineering, Southwest University, Chongqing 400715, PR China;* orcid.org/0000-0003-3664-6236

Complete contact information is available at: https://pubs.acs.org/10.1021/acsami.1c07598

Notes

The authors declare no competing financial interest.

■ ACKNOWLEDGMENTS

This work was supported by the National Natural Science Foundation of China (21775122 and 21775124) and Natural Science Foundation of Chongqing city (cstc2018jcyjAX0693), China.

■ REFERENCES

(1) Wu, D.; Sedgwick, A. C.; Gunnlaugsson, T.; Akkaya, E. U.; Yoon, J.; James, T. D. Fluorescent Chemosensors: the Past, Present and Future. *Chem. Soc. Rev.* **2017**, *46*, 7105−7123.

(2) Fan, J.; Hu, M.; Zhan, P.; Peng, X. Energy Transfer Cassettes Based on Organic Fluorophores: Construction and Applications in Ratiometric Sensing. *Chem. Soc. Rev.* **2013**, *42*, 29−43.

(3) Yi, J.-T.; Chen, T.-T.; Huo, J.; Chu, X. Nanoscale Zeolitic Imidazolate Framework-8 for Ratiometric Fluorescence Imaging of MicroRNA in Living Cells. *Anal. Chem.* **2017**, *89*, 12351−12359.

(4) Yang, Y.; Huang, J.; Yang, X.; Quan, K.; Wang, H.; Ying, L.; Xie, N.; Ou, M.; Wang, K. FRET Nanoflares for Intracellular mRNA Detection: Avoiding False Positive Signals and Minimizing Effects of System Fluctuations. *J. Am. Chem. Soc.* **2015**, *137*, 8340−8343.

(5) Hu, X.; Zhang, H.; Zhou, Y.; Liang, W.; Yuan, R.; Chen, S. A Fluorometric Lead(II) Assay by Using a DNA Dendrimer as a Carrier for the Immobilization of the Signal Probe. *Microchim. Acta* **2019**, *186*, 582.

(6) Wang, A.; Lin, Q.; Liu, S.; Li, J.; Wang, J.; Quan, K.; Yang, X.; Huang, J.; Wang, K. Aptamer-Tethered Self-Assembled FRET-Flares for microRNA Imaging in Living Cancer Cells. *Chem. Commun.* **2020**, *56*, 2463−2466.

(7) Ou, M.; Huang, J.; Yang, X.; Quan, K.; Yang, Y.; Xie, N.; Wang, K. MnO_2 Nanosheet Mediated "DD−A" FRET Binary Probes for Sensitive Detection of Intracellular mRNA. *Chem. Sci.* **2017**, *8*, 668−673.

(8) Wang, J.; Wang, D.-X.; Ma, J.-Y.; Wang, Y.-X.; Kong, D.-M. Three-Dimensional DNA Nanostructures to Improve the Hyperbranched Hybridization Chain Reaction. *Chem. Sci.* **2019**, *10*, 9758.

(9) He, L.; Lu, D.; Liang, H.; Xie, S.; Zhang, X.; Liu, Q.; Yuan, Q.; Tan, W. mRNA-Initiated, Three-Dimensional DNA Amplifier Able to Function inside Living Cells. *J. Am. Chem. Soc.* **2018**, *140*, 258−263.

(10) Lee, H.; Lytton-Jean, A. K. R.; Chen, Y.; Love, K. T.; Park, A. I.; Karagiannis, E. D.; Sehgal, A.; Querbes, W.; Zurenko, C. S.; Jayaraman, M.; Peng, C. G.; Charisse, K.; Borodovsky, A.; Manoharan, M.; Donahoe, J. S.; Truelove, J.; Nahrendorf, M.; Langer, R.; Anderson, D. G. Molecularly Self-Assembled Nucleic Acid Nanoparticles for Targeted in Vivo siRNA Delivery. *Nat. Nanotechnol.* **2012**, *7*, 389.

(11) Chatterjee, G.; Dalchau, N.; Muscat, R. A.; Phillips, A.; Seelig, G. A Spatially Localized Architecture for Fast and Modular DNA Computing. *Nat. Nanotechnol.* **2017**, *12*, 920−927.

(12) Zhang, P.; Lin, Z.; Zhuo, Y.; Yuan, R.; Chai, Y. Dual microRNAs-Fueled DNA Nanogears: A Case of Regenerated Strategy for Multiple Electrochemiluminescence Detection of microRNAs with Single Luminophore. *Anal. Chem.* **2017**, *89*, 1338−1345.

(13) Wei, Q.; Huang, J.; Li, J.; Wang, J.; Yang, X.; Liu, J.; Wang, K. A DNA Nanowire Based Localized Catalytic Hairpin Assembly Reaction for microRNA Imaging in Live Cells. *Chem. Sci.* **2018**, *9*, 7802−7808.

(14) Ren, K.; Xu, Y.; Liu, Y.; Yang, M.; Ju, H. A Responsive "Nano String Light" for Highly Efficient mRNA Imaging in Living Cells via Accelerated DNA Cascade Reaction. *ACS Nano* **2018**, *12*, 263−271.

(15) Qing, Z.; Hu, J.; Xu, J.; Zou, Z.; Lei, Y.; Qing, T.; Yang, R. An Intramolecular Catalytic Hairpin Assembly on a DNA Tetrahedron for mRNA Imaging in Living Cells: Improving Reaction Kinetics and Signal Stability. *Chem. Sci.* **2020**, *11*, 1985−1990.

(16) Zhou, R.; Yang, G.; Guo, X.; Zhou, Q.; Lei, J.; Shi, Y. Recognition of the Amyloid Precursor Protein by Human γ-Secretase. *Science* **2019**, *363*, No. eaaw0930.

(17) Alzheimer's Association. 2020 Alzheimer's Disease Facts and Figures. *Alzheimer's Dementia* **2020**, *16*, 391−460.

(18) Gong, L.; Zhang, X.; Ge, K.; Yin, Y.; Machuki, J. O. a.; Yang, Y.; Shi, H.; Geng, D.; Gao, F. Carbon Nitride-Based Nanocaptor: An Intelligent Nanosystem with Metal Ions Chelating Effect for Enhanced Magnetic Targeting Phototherapy of Alzheimer's Disease. *Biomaterials* **2021**, *267*, 120483.
(19) Liu, L.; He, Q.; Zhao, F.; Xia, N.; Liu, H.; Li, S.; Liu, R.; Zhang, H. Competitive Electrochemical Immunoassay for Detection of β-Amyloid (1−42) and Total β-Amyloid Peptides Using p-Aminophenol Redox Cycling. *Biosens. Bioelectron.* **2014**, *51*, 208−212.
(20) Zhao, Y.; Li, X.; Yang, Y.; Si, S.; Deng, C.; Wu, H. A Simple Aptasensor for Aβ_{40} Oligomers Based on Tunable Mismatched Base Pairs of dsDNA and Graphene Oxide. *Biosens. Bioelectron.* **2020**, *149*, 111840.
(21) Chan, H.-N.; Xu, D.; Ho, S.-L.; He, D.; Wong, M. S.; Li, H.-W. Highly Sensitive Quantification of Alzheimer's Disease Biomarkers by Aptamer-Assisted Amplification. *Theranostics* **2019**, *9*, 2939−2949.
(22) Fang, H.; Xie, N.; Ou, M.; Huang, J.; Li, W.; Wang, Q.; Liu, J.; Yang, X.; Wang, K. Detection of Nucleic Acids in Complex Samples via Magnetic Microbead-Assisted Catalyzed Hairpin Assembly and "DD-A" FRET. *Anal. Chem.* **2018**, *90*, 7164−7170.
(23) Bastiaens, P. I. H.; Squire, A. Fluorescence Lifetime Imaging Microscopy: Spatial Resolution of Biochemical Processes in the Cell. *Trends Cell Biol.* **1999**, *9*, 48−52.
(24) Kim, J. A.; Kim, M.; Kang, S. M.; Lim, K. T.; Kim, T. S.; Kang, J. Y. Magnetic Bead Droplet Immunoassay of Oligomer Amyloid β for the Diagnosis of Alzheimer's Disease Using Micropillars to Enhance the Stability of the Oil−water Interface. *Biosens. Bioelectron.* **2015**, *67*, 724−732.
(25) Zhou, Y.; Zhang, H.; Liu, L.; Li, C.; Chang, Z.; Zhu, X.; Ye, B.; Xu, M. Fabrication of an Antibody-Aptamer Sandwich Assay for Electrochemical Evaluation of Levels of β-Amyloid Oligomers. *Sci. Rep.* **2016**, *6*, 35186.
(26) Xia, N.; Wang, X.; Zhou, B.; Wu, Y.; Mao, W.; Liu, L. Electrochemical Detection of Amyloid-β Oligomers Based on the Signal Amplification of a Network of Silver Nanoparticles. *ACS Appl. Mater. Interfaces* **2016**, *8*, 19303−19311.
(27) Li, H.; Xie, H.; Cao, Y.; Ding, X.; Yin, Y.; Li, G. A General Way to Assay Protein by Coupling Peptide with Signal Reporter via Supermolecule Formation. *Anal. Chem.* **2013**, *85*, 1047−1052.
(28) Deng, C.; Liu, H.; Zhang, M.; Deng, H.; Lei, C.; Shen, L.; Jiao, B.; Tu, Q.; Jin, Y.; Xiang, L.; Deng, W.; Xie, Y.; Xiang, J. Light-Up Nonthiolated Aptasensor for Low-Mass, Soluble Amyloid-β_{40} Oligomers at High Salt Concentrations. *Anal. Chem.* **2018**, *90*, 1710−1717.
(29) Xia, N.; Liu, L.; Harrington, M. G.; Wang, J.; Zhou, F. Regenerable and Simultaneous Surface Plasmon Resonance Detection of A(1-40) and A(1-42) Peptides in Cerebrospinal Fluids with Signal Amplification by Streptavidin Conjugated to an N-Terminus-Specific Antibody. *Anal. Chem.* **2010**, *82*, 10151−10157.
(30) Zhou, J.; Meng, L.; Ye, W.; Wang, Q.; Geng, S.; Sun, C. A Sensitive Detection Assay Based on Signal Amplification Technology for Alzheimer's Disease's Early Biomarker in Exosome. *Anal. Chim. Acta* **2018**, *1022*, 124−130.
(31) Xia, N.; Zhou, B.; Huang, N.; Jiang, M.; Zhang, J.; Liu, L. Visual and Fluorescent Assays for Selective Detection of Beta-Amyloid Oligomers Based on the Inner Filter Effect of Gold Nanoparticles on the Fluorescence of CdTe Quantum Dots. *Biosens. Bioelectron.* **2016**, *85*, 625−632.
(32) Yin, Y.; Chen, G.; Gong, L.; Ge, K.; Pan, W.; Li, N.; Machuki, J. O. a.; Yu, Y.; Geng, D.; Dong, H.; Gao, F. DNAzyme-Powered Three-Dimensional DNA Walker Nanoprobe for Detection Amyloid β-Peptide Oligomer in Living Cells and in Vivo. *Anal. Chem.* **2020**, *92*, 9247−9256.

https://doi.org/10.1021/acsami.1c07598
ACS Appl. Mater. Interfaces 2021, 13, 32013−32021